Author Manuscript

Author Manuscript

Author Manuscript

Author Manuscript

HHS Public Access

Author manuscript

Sci Signal. Author manuscript; available in PMC 2019 September 05.

Published in final edited form as:

Sci Signal. ; 11(561): . doi:10.1126/scisignal.aat0358.

ORAI1, stromal interaction molecules 1/2, and ryanodine receptor type 1 shape sub-second Ca^{2+} microdomains upon T cell activation

B.-P. Diercks[1], **R. Werner**[2], **P. Weidemüller**[1], **F. Czarniak**[1], **L. Hernandez**[1], **C. Lehmann**[1], **A. Rosche**[1], **A. Krüger**[1], **U. Kaufmann**[3], **M. Vaeth**[3], **A. V. Failla**[4], **B. Zobiak**[4], **F. I. Kandil**[2], **D. Schetelig**[2], **A. Ruthenbeck**[5], **C. Meier**[5], **D. Lodygin**[6], **A. Flügel**[6], **D. Ren**[7], **I. M.A. Wolf**[1,†], **S. Feske**[3], **A. H. Guse**[1,*,†]

[1]The Calcium Signaling Group, Dept. of Biochemistry and Molecular Cell Biology, University Medical Centre Hamburg-Eppendorf, Germany.

[2]Dept of Computational Neuroscience, University Medical Centre Hamburg-Eppendorf, Germany.

[3]Dept of Pathology, New York University School of Medicine, USA.

[4]Microscopy Core Facility, University Medical Centre Hamburg-Eppendorf, Germany.

[5]Organic Chemistry, University of Hamburg, Germany.

[6]Institute of Neuroimmunology, University of Göttingen, Germany.

[7]Dept of Biology, University of Pennsylvania, Philadelphia, USA.

Abstract

The earliest intracellular signals determined in T cell activation are local, sub-second Ca^{2+} microdomains (1). Here we identify a Ca^{2+} entry component involved in Ca^{2+} microdomain formation in both non-stimulated and stimulated cells. In non-stimulated cells, spontaneous small Ca^{2+} microdomains depend on expression of ORAI1, STIM1, and STIM2. Using T cells stably transfected with ORAI1 fused to a genetically encoded Ca^{2+} indicator for optical imaging spontaneous Ca^{2+} microdomains depending on ORAI1 were also detected. Super resolution microscopy of non-stimulated T cells resulted in identification of a circular subplasmalemmal region with a diameter of approx. 300 nm with preformed patches of co-localized ORAI1, ryanodine receptors (RYR), and STIM1. Preformed complexes of STIM1 and ORAI1 in non-

[*]corresponding author: Andreas H. Guse, Dept of Biochemistry and Molecular Cell Biology, University Medical Centre Hamburg-Eppendorf, Martinistrasse 52, 20246 Hamburg, Germany, guse@uke.de; Phone ++49-40-7410-52828.

[†]equal contribution

Author contributions

B-PD contributed to designing this study, carried out experiments, analyzed data, prepared figures and wrote part of the manuscript. RW, FK, and DS developed and applied software components for image data analyses. PW, FC, LH, CL, AR, AK, UK, MV, AVF, BZ, FIK, DL, AR conducted experiments and analyzed data. CM, AF, DR, and SF provided reagents, helped plan and interpret experiments and wrote parts of the manuscript. IMAW contributed to designing this study, analyzed data, prepared figures and wrote part of the manuscript. AHG designed the concept of this study and wrote major parts of the manuscript.

Author Information/Competing interests

Source data are available upon request from the corresponding author.

SF is a cofounder of Calcimedica. All other authors declare that they do not have any competing financial interests.

Author Manuscript Author Manuscript Author Manuscript Author Manuscript

stimulated cells were confirmed by co-immunoprecipitation and Förster resonance energy transfer studies.

Furthermore, within the first second of T cell receptor (TCR) stimulation, Ca^{2+} microdomain numbers increase in the subplasmalemmal space, an effect not observed upon genetic deletion of *Orai1*, *Stim2* or *Ryr1* or upon antagonism of the Ca^{2+} mobilizing second messenger nicotinic acid adenine dinucleotide phosphate (NAADP).

Taken together, while preformed clusters of STIM and ORAI1 allow for local Ca^{2+} entry events in non-stimulated cells, upon TCR activation, NAADP-evoked Ca^{2+} release via RYR1, in tight interplay with Ca^{2+} entry via ORAI1 and STIM, rapidly increases the number of Ca^{2+} microdomains, thereby initiating spread of Ca^{2+} signals deeper into the cytoplasm to promote full T cell activation.

One Sentence Summary

In T cells, initial Ca^{2+} microdomains are evoked by preformed clusters of ORAI and STIM in a tight interplay with RyR1.

Introduction

In non-excitable cells such as T cells sustained Ca^{2+} signaling is mediated by store-operated Ca^{2+} entry (SOCE) that consists of two phases: upon T cell receptor (TCR) stimulation, second messengers nicotinic acid adenine dinucleotide phosphate (NAADP), D-*myo*-inositol 1,4,5-triphosphate (IP_3) and cyclic ADP-ribose (cADPR) are formed sequentially and bind to their respective target Ca^{2+} channels, such as ryanodine receptors (RyR) and IP_3 receptors (IP_3R), located in the ER (2–4). These Ca^{2+} channels open and ER-derived Ca^{2+} signals in the cytoplasm occur. The concurrent decrease of Ca^{2+} concentrations in the ER is sensed by stromal interaction molecule (STIM) 1 and STIM2 that undergo conformational changes and activate ORAI1 and ORAI2 channels in the plasma membrane (PM) resulting in SOCE (5–8).

T cell activation is initiated by cell-cell contact with an antigen–presenting cell (APC). Then, ligation of the T cell receptor/CD3 complex by major histocompatibility complex (MHC) molecules evokes juxtacrine signaling. The first intracellular signals occurring within tens and hundreds of milliseconds are local Ca^{2+} release events, termed Ca^{2+} microdomains (1, reviewed in 9). Using a high-resolution live-cell-imaging technique, we recently showed that RYR1 and NAADP are important players in local Ca^{2+} release events, called Ca^{2+} microdomains, early during T cell activation, (1). Besides RyR1, Ca^{2+} entry also contributes to Ca^{2+} microdomain formation as shown in T cells in nominally Ca^{2+}-free extracellular solution (1).

Goal of this study was molecular identification of the Ca^{2+} entry component involved in the sub-second time window following TCR stimulation. Further, we aimed to elucidate the mechanism underlying transition from non-stimulated to stimulated T cells with respect to Ca^{2+} signaling.

Author Manuscript Author Manuscript Author Manuscript Author Manuscript

Results

Using high-resolution Ca^{2+} imaging (1) in non-stimulated wildtype (wt) T cells, infrequent small Ca^{2+} microdomains occurred spontaneously close to the PM (Fig 1A, upper panel, arrow heads). These spontaneous Ca^{2+} microdomains are characterized by an amplitude of 290 ± 12 nM (mean ± SEM, n=69) and a frequency of approx. 4 signals/s per cell (Fig 1B). In contrast, in primary *Orai1*$^{-/-}$ and *Stim1*$^{-/-}$/*Stim2*$^{-/-}$ T cells, less cells displayed spontaneous Ca^{2+} microdomains and the number of such Ca^{2+} microdomains was markedly and significantly decreased (Fig 1A, B). Interestingly, in *Ryr1*$^{-/-}$ T cells number and amplitude of Ca^{2+} microdomains was not different from wt cells (Fig 1A, D). Moreover, blockade of NAADP evoked Ca^{2+} release by the specific antagonist BZ194 (10) did not alter spontaneous Ca^{2+} microdomains, indicating that the NAADP/RYR1 signaling axis is not involved in spontaneous Ca^{2+} microdomains.

Further, subsecond kinetics of spontaneous Ca^{2+} microdomain formation was analyzed in the subplasmalemmal space. The analyzed layer is ~ 423 ± 32 nm (mean ± SD, n= 206) in depth and comprises an area spanning a 90° angle of the confocal plane analyzed (Fig 1 C, D, insets; for analysis of T cells using dartboard segments see also suppl Fig S1). In this layer, almost no Ca^{2+} microdomains were present in *Orai1* and *Stim1/2*-deficient T cells, which differs significantly from wt T cells (Fig 1 C). In contrast, no significant inhibitory effect of *Ryr1* deletion on spontaneous subplasmalemmal Ca^{2+} microdomains was observed (Fig 1A lower panel, D). Consistently, a marked and statistically significant difference in the mean free cytosolic Ca^{2+} concentration ($[Ca^{2+}]_i$) was observed between wt and *Orai1*$^{-/-}$ or *Stim1*$^{-/-}$/*Stim2*$^{-/-}$ quiescent T cells (20±3 nM, n=68, vs 14±2nM or 5±2 nM, n= 45, $p<0.001$, Kruskal-Wallis test), but not between wt and *Ryr1*$^{-/-}$ T cells (28±3nM, n=67, vs 22±5nM, n=31, $p>0.05$, Kruskal-Wallis test). These results again suggest basal Ca^{2+} entry driven microdomains by pre-activated ORAI1 and STIM1/STIM2 clusters of non-stimulated T cells, while RYR1 or NAADP do not appear to be of major importance in this process.

As independent approach, spontaneous Ca^{2+} microdomains were analyzed in Jurkat T cells stably transfected with ORAI1 fused to a genetically encoded Ca^{2+} indicator for optical imaging (GECO) (Fig 2), that detects Ca^{2+} entry via ORAI1 channels (11). Spontaneous local and oscillatory Ca^{2+} entry events via ORAI1 were observed in the presence of 1 mM extracellular Ca^{2+} (Fig 2 A, B upper panels). Chelating free extracellular Ca^{2+} with EGTA markedly decreased these spontaneous Ca^{2+} entry events (Fig 2 A, B, 2nd upper panels). Involvement of ORAI1 was further confirmed by inhibiting Ca^{2+} entry using the specific CRAC channel inhibitor Synta 66 (Fig 2 A, B, middle panels). Rapid chelation of free cytosolic Ca^{2+} by pre-loading the cells with 5 μM BATPA-AM also largely diminished ORAI1-GECO signals, indicating that the freely diffusible BAPTA free acid competes effectively with the GECO construct for free Ca^{2+} ions entering the cell through ORAI1 (Fig 2 A, B, 2nd lower panels). Inhibition of NAADP signaling by BZ194 (10) had no effect on spontaneous Ca^{2+} microdomains (Fig 2 A, B, bottom panels). Quantification of spontaneous local Ca^{2+} entry events at 4 different ROIs revealed significant decreases in the absence of extracellular Ca^{2+}, buffering of free cytosolic Ca^{2+} with BATPA or upon inhibition by Synta 66 (Fig 2 C), confirming Ca^{2+} microdomain data in Fig 1 and further suggesting that

Author Manuscript Author Manuscript Author Manuscript Author Manuscript

preformed clusters of ORAI1 and STIM1 are constitutively active at single sites already in non-stimulated T cells.

To investigate preformed clustering of STIM1 and ORAI1 in non-stimulated T cells, we used (i) immunoprecipitation, (ii) Förster resonance energy transfer (FRET), or (iii) stimulated emission-depletion (STED) super resolution confocal microscopy (Fig. 3). Pull down of fragmented membranes obtained from Jurkat T cells using beads coupled with either anti-ORAI1 or anti-STIM1 were then subjected to SDS-PAGE and further western blotted using anti-STIM1 and anti-ORAI1 (Fig 3 A to C). In positive controls stimulated with thapsigargin (+Tg) for 10 min, clear western signals were obtained for ORAI1 in case of STIM1 pull down, and for STIM1 in case of ORAI1 pull down (Fig. 3B). In non-stimulated control samples (-Tg), much weaker, but clearly detectable signals were obtained suggesting preformed STIM1/ORAI1 clusters in non-stimulated Jurkat T cells (Fig. 3B). Similarly, in non-stimulated primary wt T cells, Orai1 was detected after pull down with anti-STIM1 (Fig 3 C, D). Using FRET the formation of functional STIM1-ORAI1 complexes was further verified. After correction for spectral crosstalk (bleed-through) and stray-light removal, FRET signals were detected in non-stimulated Jurkat T cells at the plasma membrane (Fig 3E upper panel, F). These signals were strongly increased upon stimulation with Tg for 10 min (Fig 3E lower panel, F). STED super resolution confocal microscopy with 40 nm spatial resolution (xy dimension; suppl Fig S2) revealed plasma membrane/subplasma membrane areas (Fig3 GH) with either strong co-localization of STIM1 and ORAI1 (Fig 3G, panel ‘merge’, region1) or with ORAI1 alone (Fig 3G, panel ‘merge’, region2). While those areas without co-localization of ORAI1 and STIM1 are unlikely to play major roles for the spontaneous Ca^{2+} microdomains, patches of strong co-localization of STIM1 and ORAI1 at the PM of non-stimulated primary T cells very likely are the sites of such events. These patches had a length of ~ 1 μm and penetrated ~ 300 nm into the cytoplasm (Fig 3 I). Within these patches, STIM1 and ORAI1 clusters were adjacent and partially overlapped with a high co-localization coefficient of 0.61 ± 0.03 (mean ± SEM, n=17) (Fig 3 G–J). The close co-localization of ORAI1 and STIM1 in non-stimulated cells complements immunoprecipitation and FRET data described above and substantiates a functional interaction between STIM1 and ORAI1 in spontaneous Ca^{2+} microdomains at ER-PM junctions.

Stimulation of wt T cells using microbeads coated with anti-CD3 and anti-CD28 mAb resulted in an immediate increase of number and amplitude of small Ca^{2+} microdomains within the first 15 s of stimulation while at approx. 25 s global Ca^{2+} signaling began (Fig 4A upper panel, suppl movie S1). Regions-of-interest (ROI) set below the PM, in the cytosol, or in the nucleus, indicate a rapid increase of $[Ca^{2+}]_i$ below the PM at site of stimulation followed by similar increases nearby in the cytosol, while at the opposite side of the cell below the plasma membrane or in the nucleus Ca^{2+} microdomains were not detected within 15 s (Fig 4B). In contrast to wt T cells, in *Orai1*$^{-/-}$ T cells almost no Ca^{2+} microdomains were observed (Fig 4A lower panel, 4C; suppl movie S2). In the few cases where Ca^{2+} microdomains were recorded in *Orai1*$^{-/-}$ T cells, they preferentially occurred more deeply within the cytosol (suppl Fig S3). Significant and strong impairment of Ca^{2+} microdomain numbers within 15s post TCR/CD28 stimulation was not only observed in *Orai1*$^{-/-}$ T cells, but similar results were obtained in T cells from *Stim2*$^{-/-}$ and *Stim1*$^{-/-}$/*Stim2*$^{-/-}$ mice (Fig

Author Manuscript Author Manuscript Author Manuscript Author Manuscript

4D left panel, movie S3). Further, for *Orai1*$^{-/-}$ or *Stim1*$^{-/-}$/*Stim2*$^{-/-}$ T cells there was also a significant decrease in the amplitude of the microdomains (Fig 4D right panel). Representative examples for *Stim1*$^{-/-}$, *Stim2*$^{-/-}$ or *Stim1*$^{-/-}$/*Stim2*$^{-/-}$ T cells demonstrate the largely diminished number and amplitude of Ca^{2+} microdomains (suppl Fig S4). This effect is also reflected by the so-called 'dartboard'projection (principle shown in suppl Fig S1) where the confocal plane analyzed in each cell is split into segments of identical area, each displaying the mean number of local Ca^{2+} signals in color-coded fashion (suppl Fig S5).

In *Stim1*$^{-/-}$ T cells, the number of Ca^{2+} microdomains per cell was slightly, but not significantly decreased within the first 15 s, whereas *Stim2*$^{-/-}$ T cells showed a significant reduction (Fig 4D). Further, in *Stim1*$^{-/-}$/*Stim2*$^{-/-}$ T cells the percentage of cells responding with ≥1 microdomain within 15 s post stimulation dropped from 78% (control) to 18%. No difference in the number of Ca^{2+} microdomains was observed in T cells upon deletion of *Orai2*, although ORAI2 was shown to synergize with ORAI1 to mediate SOCE after store depletion (*8;* suppl Fig S6).

How do Ca^{2+} microdomains occur and spatio-temporally propagate within activated T cells? To address this question, subsecond kinetics of Ca^{2+} microdomain formation *following* T cell activation were analyzed below the PM of T cells close to the site of TCR/CD28 stimulation. The numbers of Ca^{2+} microdomains (calculated per cell and frame) increased ~100 ms post TCR/CD28 stimulation in wt T cells (Fig 4E). Comparison of wt vs *Orai1*$^{-/-}$, *Stim1*$^{-/-}$, *Stim2*$^{-/-}$ and *Stim1*$^{-/-}$/*Stim2*$^{-/-}$ T cells revealed significantly decreased Ca^{2+} microdomain numbers as soon as 100 ms post TCR stimulation (Fig 4E). To elucidate potentially differential role(s) of STIM1 vs STIM2 in this initial phase of T cell activation, Ca^{2+} microdomain formation was analyzed in temporal segments, either before stimulation, or in 5s-segments post stimulation (Fig 4F). Before stimulation and within the first 5s post stimulation all *Stim1*$^{-/-}$, *Stim2*$^{-/-}$ or *Stim1*$^{-/-}$/*Stim2*$^{-/-}$ T cells showed markedly decreased numbers of Ca^{2+} microdomains (Fig 4F). This effect was stronger and statistically significant for *Stim2*$^{-/-}$ and *Stim1*$^{-/-}$/*Stim2*$^{-/-}$ T cells within 5 s post stimulation. Within the next four 5s-segments, knockout of *Stim1*$^{-/-}$ gradually became less severe regarding Ca^{2+} microdomain numbers, while *Stim1*$^{-/-}$/*Stim2*$^{-/-}$ T cells had the same largely and significantly reduced numbers of Ca^{2+} microdomains (Fig. 4F), suggesting that knockout of STIM1 was functionally more and more replaced by STIM2. Between 55 to 60s in both single knock-outs, either *Stim1*$^{-/-}$ or *Stim2*$^{-/-}$, Ca^{2+} microdomain formation was indistinguishable from wt cells (Fig. 4F), suggesting that at this later time point both STIM proteins may replace each other, while the phenotype of the *Stim1*$^{-/-}$/*Stim2*$^{-/-}$ double knockout was similarly severe for all temporal segments (Fig. 4F).

We next asked how Ca^{2+} release and entry systems cooperate to form Ca^{2+} microdomains. In previous work, we suggested RYR1, possibly activated by NAADP, to be the main Ca^{2+} release channel involved in Ca^{2+} microdomain formation upon TCR/CD28 stimulation (1). Here, we confirm this finding showing that the percentage of responding cells as well as the number of microdomains per cell in the first 15 s of T cell activation was decreased in *Ryr1*$^{-/-}$ cells (Fig 5A). Subsecond kinetics of $[Ca^{2+}]_i$ for T cells from *Ryr1*$^{-/-}$ mice also revealed significantly less Ca^{2+} microdomains in the first second following TCR/CD28

Author Manuscript Author Manuscript Author Manuscript Author Manuscript

stimulation compared to wt control T cells (Fig 5B). Similarly, blocking NAADP signaling using NAADP-antagonist BZ194 (10) resulted in significantly decreased percentage of responding cells as well as decreased number of Ca^{2+} microdomains in the first 15 s of T cell activation (Fig 5C). Subsecond kinetics of Ca^{2+} microdomain formation provides further evidence for NAADP acting in this early time period (Fig 5 D).

Since also two-pore channels 1 and 2 (TPC1 and 2) were proposed to respond to NAADP (12–14), tested them and also RYR3 as further candidates regarding potential roles in the formation of spontaneous or antigen receptor-triggered Ca^{2+}microdomains. However, in T cells with deletions of both *Tpc1* and *Tpc2,* neither the percentage of responding cells, the number of Ca^{2+} microdomains, nor their amplitude was altered upon TCR/CD28 stimulation (Fig 5E). Similarly, genetic deletion of *Ryr3* did not alter these Ca^{2+} microdomain parameters upon TCR/CD28 stimulation (Fig 5F). Then, we hypothesized that the close functional interaction of RYR1 and ORAI1 proposed here, requires co-localization of these proteins. STED super resolution microscopy revealed such co-localization of RYR and ORAI1 in patches at or very close below the plasma membrane (Fig 4G–J). The extent of co-localization between RYR and ORAI1 and STIM1 and ORAI1 in these patches was similar with co-localization coefficients of 0.70 ± 0.05 and 0.61 ± 0.03, respectively (Fig 4J, Fig 3J). It is noteworthy that co-localization of ORAI1, RyR and STIM1 occurred in some, but not all regions of the PM (compare Fig H2(2) vs Fig 4H(2)), which is likely due to the fact that the most likely sites for such interactions, the ER-PM junctions, cover only a fraction of the PM (15).

Discussion

Here, we identified and characterized for the first time spontaneous Ca^{2+} microdomains below the plasma membrane of non-stimulated T cells, with amplitudes of 290 ± 12 nM (mean ± SEM, n=69) and a frequency of approx. 4 signals/s per cell. These spontaneous Ca^{2+} microdomains depend on ORAI1 and both STIM1 and STIM2. Preformed complexes of ORAI1 and STIM1 in non-stimulated T cells were detected using immunoprecipitation, FRET and STED microscopy. Thus, preformed complexes of ORAI1 and both STIM1 and STIM2 constitute a system allowing for continuous low level Ca^{2+} entry, resulting in a ‘basic excitability’ of naïve T cells (suppl Fig S7). In the early phase post stimulation of TCR/CD28, a second system consisting of the second messenger NAADP and RYR1 comes into play. Ca^{2+} release via RYR1 at PM – ER junctions results in an increased number of Ca^{2+} microdomains and the concomitant decrease of the luminal Ca^{2+} concentration of the ER leads to enhanced recruitment and activation of STIM/ORAI1 complexes, thereby further enhancing Ca^{2+} microdomains (suppl. Fig S7).

Spontaneous Ca^{2+} microdomains

Detection of Ca^{2+} microdomains require Ca^{2+} imaging system with high spatial and temporal resolution and a very good signal-to-noise ratio for the Ca^{2+} signal. The detection limit of the system used here is approx. 113 nM regarding Ca^{2+} amplitude (see details in Methods section); an image acquisition rate of $40s^{-1}$ at 368 nm spatial resolution well

Author Manuscript Author Manuscript Author Manuscript Author Manuscript

allowed for detection and characterization of both spontaneous and stimulation-dependent Ca^{2+} microdomains.

In other cells types, spontaneous Ca^{2+} microdomains are best studied in cardiac myocytes (16,17) or astrocytes (18–21). In cardiac myocytes, RYR2 is the major Ca^{2+} release channel that amplifies low, plasma membrane-near Ca^{2+} signals originating from activation of L-type Ca^{2+} channels (LTCC). RYR2 and LTCC are spatially organized in couplons. In cardiac myocytes from end-stage heart failure patients, spontaneous Ca^{2+} microdomains were observed in the vicinity of RYR2 localized outside of such couplons, e.g. outside the transverse and axial tubular system (16). Using second harmonic generation and 2-photon-fluorescence, Ca^{2+} microdomains generated by RYR2 as well as local sarcomere contractions were analyzed, resulting in detection of locally coordinated Ca^{2+} sparks and contractions (17). Although the ER in T cells is not as much ordered as the sarcoplasmic reticulum in cardiac myocytes, we observed alternating patches of RYR and ORAI1 at or very close below the plasma membrane (Fig 4G–J), indicating that proper localization of RYR may in general be an important mechanism for regulation of Ca^{2+} microdomains.

In astrocytes, spontaneous Ca^{2+} microdomains with unknown function were described (18), either as a result of brief openings of the mitochondrial permeability transition pore (19), or by Ca^{2+} entry across the extracellular space (20), thus mechanistically resembling the system described here for non-stimulated T cells. Interestingly, it was, recently hypothesized that Ca^{2+}microdomains are the local regulatory units of astrocyte interaction with other cell types, e.g. neurons (21).

Preformed STIM/ORAI1 complexes

While in the classical model of capacitative Ca^{2+} entry a substantial decrease of luminal Ca^{2+} concentration in the ER ($[Ca^{2+}]_{lu}$) is required for ORAI1 activation by STIM1, there is more and more evidence that STIM2 is pre-clustered close to the plasma membrane and activates ORAI1 constitutively, at least in overexpressing cells (22–26). Since in non-stimulated cells $[Ca^{2+}]_{lu}$ is relatively high, only STIM2, due to its lower affinity for Ca^{2+}, is able to sense small decreases of $[Ca^{2+}]_{lu}$, that may occur in non-stimulated cells, in cells stimulated by low agonist concentration, or at the very start of stimulation, as in the present study. In this context, STIM2 was recently shown to enhance the sensitivity of ORAI1 activation at relatively high $[Ca^{2+}]_{lu}$ by promoting STIM1 clustering in ER-PM junctions (27). The underlying mechanism was also very recently reported: by remodeling the C-terminus of STIM1 to an activated conformation, STIM2 traps STIM1at ER-PM junctions to cause STIM1 coupling to ORAI1, thereby facilitating enhanced Ca^{2+} entry (28). Accordingly, a model with 3 different states was proposed: (i) STIM2-ORAI1 clustering at ER-PM junctions at relatively high $[Ca^{2+}]_{lu}$, (ii) recruitment of STIM1 by STIM2 resulting in STIM2-STIM1-ORAI1 clustering, and (iii) replacement of STIM2 in this ternary complex by STIM1 for full activation of ORAI1 at lower $[Ca^{2+}]_{lu}$ (28). When applying this model to spontaneous Ca^{2+} microdomains and stimulated very early microdomain formation in primary T cells, the second state with STIM2-STIM1-ORAI1 clustering appears most likely, since before and in the first 5s post TCR/CD28 stimulation single knock-outs of *Stim2* and *Stim1* cause a similar decrease of Ca^{2+} microdomains as the double knock-out (Fig. 4 F).

Author Manuscript Author Manuscript Author Manuscript Author Manuscript

Between 5 and approx. 20 s post TCR/CD28 stimulation, *Stim1* knockout gradually shows a less severe phenotype indicating that during this phase STIM2 is able to substitute for STIM1 (Fig. 4 F). At later time points (25–60s) the strong dependency on STIM2 also gradually decreases, indicating that both STIM1-ORAI1 complexes or STIM2-ORAI1 complexes are sufficient to promote Ca^{2+} microdomains and beginning global Ca^{2+} signaling. Why STIM2 is able to substitute for STIM1 between 5 and approx. 20 s post TCR/CD28 stimulation cannot be explained presently and will be object of future investigation.

No role for TPC1/2 or RYR3 in Ca^{2+} microdomains

In addition to identification of the rapid Ca^{2+} entry component, we also re-analyzed rapid Ca^{2+} release involved in Ca^{2+} microdomain formation. We confirm here RYR1 as major Ca^{2+} release channel in this process (Fig 5), as described in (1). Furthermore, we demonstrate that NAADP antagonism is an effective way to suppress antigen receptor-triggered Ca^{2+} microdomain formation, while spontaneous Ca^{2+} microdomains were not affected by NAADP antagonist BZ194. Together with our recent data that NAADP does not evoke Ca^{2+} microdomains in T cells lacking RYR (1), and with single channel recordings demonstrating activation of RYR1 by NAADP (29), we hypothesize that NAADP is formed very rapidly and activates Ca^{2+} release via RYR1 (supp Fig 7). In our recent work, TRPM2 was excluded as potential NAADP target (1). Here, we exclude other potential NAADP target candidates, TPC1 and TPC2, by demonstrating no effect of a functional double knock-out of these endo-lysosomal ion channels (Fig 5). These results are in accordance with previous findings that TPC1/2 are unrelated Na^{+} channels activated by phosphatidylinositol 3,5-bisphosphate or regulated in an ATP-dependent fashion by mTOR (30, 31).

Likewise, knock-out of RYR3 did not affect Ca^{2+} microdomain formation in primary T cells (Fig 5). However, it is possible that RYR3 plays an important role in Ca^{2+} signaling at later stages of T cell activation, for instance in Ca^{2+} induced Ca^{2+} release (CICR) and cADPR signaling (3, 32).

Taken together, we propose a new model for formation of initial Ca^{2+} microdomains in T cells (suppl fig S7). In non-stimulated T cells, ORAI1 and STIM1/STIM2 form protein complexes at ER-PM contact sites resulting in discrete, local Ca^{2+} entry signals (suppl Fig S7). These constitutive Ca^{2+} microdomains do not further propagate without cell activation, e.g. due to Ca^{2+} buffering or lowering of $[Ca^{2+}]_i$ by Ca^{2+} ATPases in ER or PM. The preformed ORAI1-STIM1/STIM2 complexes suggest that the SOCE machinery in T cells is poised to respond very quickly to TCR stimulation. Preformed ORAI1-STIM1 complexes are reminiscent of similar co-localization of both proteins at triad junctions of skeletal muscle fibers (33). Upon TCR stimulation, RYR1 is activated, probably by NAADP formed within a few seconds of T cell stimulation (4), resulting in local and transient Ca^{2+} release (1). This release contributes directly to Ca^{2+} microdomains and in addition promotes the activation of STIM1, STIM2 and thus SOCE through ORAI1 channels within the first second following TCR stimulation. Our findings shed new light on the intricate interaction of RYR1, ORAI1 and STIM1/STIM2, which controls Ca^{2+} signaling in T cells and thereby adaptive immune responses.

Author Manuscript Author Manuscript Author Manuscript Author Manuscript

Materials and Methods

Reagents

Fluo4-AM, Fura Red-AM and Fura2-AM were obtained from Life Technologies. Ca^{2+} indicators were dissolved in DMSO, divided into aliquots, and stored at −20 °C until required for use. Anti-mouse CD3 mAb and Anti-mouse CD28 mAb were obtained from BD Biosciences.

Synthesis of 3-carboxy-1-(2-(octylamino)-2-oxoethyl)pyridin-1-ium bromide (BZ194)

Under a dry atmosphere of nitrogen, 1.0 mL bromoacetyl bromide (11.4 mmol, 1 eq.) was dissolved in 25 mL anhydrous dichloromethane and the mixture cooled to −40 °C. Under vigorous stirring, 1.9 mL pyridine (22.9 mmol, 2 eq.) in 15 mL dichloromethane were added slowly and dropwise. The resulting suspension was stirred for further 30 min and allowed to warm up to −10 °C. Successively, 1.9 mL *n*-octylamine (11.4 mmol, 1 eq.) in 15 mL dichloromethane were added dropwise. The yellow reaction mixture was stirred for 60 min between −10 °C and room temperature. Termination of the reaction was carried out by addition of water. The biphasic mixture was diluted further with dichloromethane, and washed twice with each 1 M hydrochloric acid (aq.), sodium bicarbonate (sat., aq.) and brine. The organic layer was dried over sodium sulfate, filtrated and the solvent evaporated under reduced pressure. The resulting orange oil (2.1 g, 8.31 mmol, 73%) was dried in vacuum and the obtained 2-bromo-*N*-octylacetamide used as such in the next reaction step. In 10 mL *N*,*N*-dimethylformamide, 0.45 g nicotinic acid (3.7 mmol, 1 eq.) and 0.92 g 2-bromo-*N*-octylacetamide (3.7 mmol, 1 eq.) were reacted with another at 70 °C for 24 h. Successively, the solvent was removed under high vacuum, and the obtained residue purified by automated normal phase column chromatography using a methanol gradient against dichloromethane (0 – 10% from 0 – 20 min, isocratic from 20 – 30 min). The yellowish solid was crystallized from acetone/methanol and 3-carboxy-1-(2(octylamino)-2-oxoethyl)pyridine-1-ium bromide finally obtained as white crystals (0.67 g, 1.8 mmol, 49%).

Animal Models

The generation of $Ryr1^{-/-}$ (1), $Ryr3^{-/-}$ (34), $Tpc1^{-/-}Tpc2^{-/-}$ (30), $Orai1^{fl/fl}Cd4cre$ (herein $Orai1^{-/-}$) (35), $Orai2^{-/-}$, $Orai1^{fl/fl}Orai2^{-/-}Cd4cre$ (8), $Stim1^{fl/fl}Cd4cre$ ($Stim1^{-/-}$), $Stim2^{fl/fl}Cd4cre$ ($Stim2^{-/-}$), $Stim1^{fl/fl}Stim2^{fl/fl}Cd4cre$ ($Stim1^{-/-}2^{-/-}$) (36) has been previously described. ‘wt’ refers to C57BL/6 mice and all animals were on a C57BL/6 genetic background. Sex-matched male and female mice between 6 and 13 weeks old were used. Mice were maintained under specific pathogen-free conditions in accordance with institutional guidelines for animal welfare approved by the Institutional Animal Care and Use Committees at New York University School of Medicine, University of Göttingen, University Medical Centre Hamburg-Eppendorf, and at the University of Pennsylvania.

Generation of stable transfected Jurkat T cells with G-GECO1.2-Orai1 construct

The Orai1-G-GECO1.2 (10) (Addgene plasmid # 73562) was a gift from Michael Cahalan (University of California, Irvine). The encoding fragment of 2.3 kbp size was excised from plasmid pCMV-OraiG-GECO1.2 by AgeI/MunI digestion and cloned into AgeI and EcoRI

Author Manuscript Author Manuscript Author Manuscript Author Manuscript

sites of pF-CAG-GFP vector (derived from lentiviral pFUGW construct where Ubiqitin C promoter was exchanged by chicken actin gene promoter, CAG) replacing GFP open reading frame. Pseudoviral particles were generated by co-transfecting pF-CAG-Orai1-G-GECO1.2 construct with three packaging plasmids (3rd generation system) in HEK 293 cells using Lipofectamine 2000 reagent (Thermo Fisher) and culturing in OptiPro medium supplemented with Penicillin/Streptomycin and L-Glutamine (1:100, Thermo Fisher) for 48 h. Supernatant was cleared by centrifugation, filtered through 0.45 μm filter and added to Jurkat JMP cells for overnight incubation in the presence of 8 μg/mL polybrene (Sigma). Transduced pool of Jurkat cells was further propagated in RPMI1640 medium supplemented with 10% FCS for few passages. To enrich the population for highly expressing cells, the transduced pool was sorted on FACS Aria II flow cytometer (Becton Dickinson) after addition of thapsigargin (Sigma) to a concentration of 2 μM.

Isolation of primary T cells

CD3+ as well as CD4+ T cells were freshly isolated from spleen and lymph nodes, some of which were shipped to Hamburg/Germany on wet ice, by negative selection using the EasySep Mouse T Cell Enrichment Kit or the EasySep Mouse CD4+ T Cell Enrichment Kit (STEMCELL Technologies Inc.). Cell purity (which was typically 95% T cells) was assessed by immunostaining with fluorescein isothiocyanate–conjugated anti-mouse TCRb antibody (clone H57–597, BioLegend) and measured with a FACSCalibur flow cytometer (BD Biosciences).

Ca^{2+} imaging in primary T cells

Single cell Ca^{2+} imaging was performed as previously described (1). In brief, freshly isolated T cells were loaded with Fluo4-AM (10 μM) and Fura Red-AM (20 μM) for 50 min at RT. After washing, the cells were resuspended in Ca^{2+} buffer [140 mM NaCl, 5 mM KCl, 1 mM $MgSO_4$, 1 mM $CaCl_2$, 20mM Hepes (pH 7.4), 1mM NaH_2PO_4, 5 mM glucose]. To stimulate the T cells, Protein G Beads (Merck Millipore) were coated with antibodies (anti-CD3/anti-CD28) according to the manufacturer's instructions. Coverslips were coated with bovine serum albumin (5 mg/ml, Sigma-Aldrich) and poly-L-lysine (0.1 mg/ml, Sigma-Aldrich) to facilitate adherence of T cells. Imaging was carried out with a Leica IRBE2 microscope (100-fold magnification) using a Sutter DG-4 as a light source and an electron-multiplying charge-coupled device camera (C9100, Hamamatsu). Exposure time was 25 ms (40 fps) in 14-bit mode with two-fold binning. A Dual-View module (Optical Insights, PerkinElmer Inc.) was used to split the emission wavelengths with the following filters (ex, 480/40; bs, 495; em1, 542/50; em2, 650/57).

Fluo4/Fura Red Ca^{2+} image processing

Volocity software (version 6.6.2; PerkinElmer) was used for the image acquisition and Ca^{2+} image post-processing was done with Matlab (Mathworks) (37). First, the background in each channel was corrected. Bleaching of Fura Red was corrected using a frame-by-frame elevation of pixel intensities by the difference between the initial value and the fit value of the specific frame with an additive approach. To obtain digital confocal images Fluo4 and Fura Red were deconvolved using the Lucy-Richardson algorithm with an analytically computed Point-Spread-Function (PSF) and both fluorescence channels were automatically

Author Manuscript Author Manuscript Author Manuscript Author Manuscript

aligned by a rigid sum-of-squared-differences-based registration. In a final step the Fluo4/Fura Red ratio was generated, median filtered (3×3) and exported.

Ca^{2+} calibration

The initial mean Fura Red fluorescence (Fura Red_{t0}) was as high as the Fura Red fluorescence after correction for bleaching due to the additive frame-by-frame bleaching correction. Thus, the calculation of $[Ca^{2+}]_i$ was performed using *in situ*–determined R_{min} [$Fluo4_{min}$/Fura Red_{t0} after EGTA chelation] and R_{max} [$Fluo4_{max}$/Fura $Redt_0$] in single cell measurements. Previously determined mean K_d of Fluo4 and Fura Red of 408 ± 12 nM was used (1) and data were subjected to image post-processing.

Identification of local Ca^{2+} microdomains

Local subcellular Ca^{2+} microdomains were identified on a frame-by-frame basis and defined as small, compact connected pixel sets (minimum pixel set size: 6 pixels; maximum pixel set size: 20 pixels; minimum pixel set circularity of 0.5, with circularity defined as [4π × area of pixel set] / [perimeter of pixel set]^2) with high $[Ca^{2+}]_i$ values compared to the mean $[Ca^{2+}]_i$ value in the cell. To distinguish between background noise and Ca^{2+} microdomains, cell-free homogeneous Ca^{2+}-EGTA buffer ($[Ca^{2+}]$ = 225 nM) containing Fluo4 and Fura Red (1) was analyzed. After processing the cell-free images as described for single cell images, no (noise-induced) fictive Ca^{2+} microdomains were detected for Ca^{2+} levels of more than 112.5 nM above the cell-free buffer mean Ca^{2+} level. Hence, for Ca^{2+} microdomain detection in cell images, all pixel $[Ca^{2+}]_i$ values of the microdomain had to be at least $\Delta[Ca^{2+}]_i$ = 112.5 nM higher than the frame-specific mean $[Ca^{2+}]_i$ of the considered cell. Reported local Ca^{2+} signal values refer to maximum $[Ca^{2+}]_i$ values for the signal pixel set. Data are shown as Ca^{2+} microdomains per cell and frame.

Ca^{2+} microdomain analysis and comparison for subcellular compartments

To enable analysis and comparison of Ca^{2+} microdomains for specific subcellular divisions (e.g. “close to point of activation/bead contact”) and cell groups, a so-called “dartboard projection” approach was introduced: First, a circular, dartboard-like template (with three annuli and individual annuli layers of same area) was matched onto the individual cell images using an automated template-to-cell matching by circle Hough Transform (suppl. Fig S1). Then, based on their spatial coordinates, the identified local Ca^{2+} signals were assigned to the corresponding template layers. The resulting dartboards were normalized with respect to the location of the bead contact zone by rotating the template. Finally, the cell-specific segment-wise local Ca^{2+} signal information was aggregated and evaluated for the considered group. All Ca^{2+} analysis steps were implemented using Matlab.

Preparation of the subcellular fraction P10 and immunoprecipitation of STIM1 and ORAI1

Jurkat T cells (approx. 2×10^7 lymphocytes/experiment) were harvested, washed in Ca^{2+} buffer and homogenized on ice by mechanical disruption in an RSB buffer (pH 7.2; 20mM HEPES, 10mM NaCl, 3mM $MgCl_2$, protease inhibitors). After 20 min of centrifugation at 10,000 × g the resulting pellet (P10 fraction) was resuspended in RSB buffer. Protein concentration was assessed by Bradford Reagent (Bio-Rad) protein assay using bovine

Author Manuscript Author Manuscript Author Manuscript Author Manuscript

serum albumin as standard. 4 μg of anti-ORAI1 or anti-STIM1 mAb (ThermoFischer) were coupled to Protein G magnetic beads (over night at 4°C). After rinsing the magnetic beads, 400 μg P10 membranes were used for the pull down by gently mixing them with 50 μl of bead suspension at 4°C for 1.5 h. Protein bound to the magnetic beads was collected, washed with PBS-TWEEN (0,1%) and resuspended in standard sample buffer for reducing SDS-PAGE. Protein bound to beads was released by heating (94° C, 10 min), separated by SDS-polyacrylamide gel (12.5%) electrophoresis and transferred to PVDF membranes for Western-blot analysis (transfer conditions: 14 V, 200 mA, room temperature, 1.5 h). The blots were immunostained with both primary antibodies (anti-STIM1, 1:1000 dilution; anti-ORAI1, 1:100 dilution), incubated over night at 4°C. Proteins were visualized with secondary antibodies (incubated for 1h at RT) coupled with horseradish-peroxidase (HRP) using SuperSignal West Pico Chemiluminescent (Thermo Scientific) as substrate.

Experiments with primary T cells were done in an identical manner, except that primary murine T cells were washed in Ca^{2+} buffer and sonicated on ice (4 × 6 sec) to disintegrate the cells. For pull downs we used whole cell lysates from 3×10^7 cells (3 spleens) by gently mixing them with 50μl of bead suspension at 4 °C for 1.5 h.

FRET Imaging

Jurkat T cells were transfected with 15 μg of human STIM1 CFP and ORAI1 YFP by electroporation. Both plasmids STIM1 CFP (Addgene plasmid # 19755) and Orai1 YFP (Addgene plasmid # 19756) were gifts from Murali Prakriya (Northwestern University, Chicago) and Anjana Rao (La Jolla Institute, San Diego) (38). FRET experiments were performed with intact cells 24 hours after transfection. Imaging was carried out with a Leica IRBE microscope (100-fold magnification) using a Sutter DG-4 as a light source and two electron-multiplying charge-coupled device camera (C9100–13, Hamamatsu). Exposure time was 100 ms in 16-bit mode. A Dual-Cam-View (Optical Insights, PerkinElmer Inc.) was used to split the emission wavelengths with the following filters (CFP_{ex} 430/24; YFP_{ex} 500/20; CFP_{em} 470/24; YFP_{em} 535/20). FRET images were corrected for spectral crosstalk (bleedthrough) of the donor and acceptor signal into the FRET channel. Bleedthrough correction was determined by expressing the donor (STIM1 CFP) and acceptor (ORAI1 YFP) separately and the resulting bleed-through (CFP: 44%; YFP: 4%) was subtracted from the FRET channel image of double transfected cells, to get the true FRET image. Moreover, 75% of stray light was removed from the FRET images with Openlabś (version 5.5.2, PerkinElmer Inc.) no-neighbor deconvolution.

STED imaging

Freshly isolated primary T cells were seeded on poly-L-lysine (0.1 mg/ml, Sigma-Aldrich) coated coverslips. Fixation was done with 3% para-formaldehyde (Electron Microcopy Sciences) for 15 min. Additionally, cells were permeabilized with 0.05% saponin (v/v; Fluka) for 15 min. Primary antibodies (rabbit anti-ORAI1, 1:100 (Proteintech); mouse anti-pan-RYR, 1:100 (Santa Cruz); mouse anti-STIM1, 1:200 (Thermo Scientific)) were diluted in 3% (v/v) fetal bovine serum and incubated overnight a 4°C. Secondary antibodies (anti-rabbit STAR RED (Abberior Instruments); anti-mouse AlexaFluor 594 (Biolegend)) were incubated (1:200) for 1h at room temperature. Coverslips were mounted with Abberior

Author Manuscript Author Manuscript Author Manuscript Author Manuscript

Mount Solid (Abberior) overnight. Images were acquired with the Abberior 4-channel easy3D STED with 775 and 595 depletion beams (Abberior Instruments) equipped with a Nikon 60x time 1.4 NA objective and a QUAD beam scanner. Alexa 594 nm was excited with a pulsed 561 nm diode beam, depleted with a pulsed 775 nm STED beam and detected with a 615 ± 20 nm emission filter. Star red 640 nm was excited with a pulsed 640 nm diode beam, depleted with a pulsed 775 nm STED beam and detected with a 685 ± 70 nm emission filter. The pixel size was set to 20 nm. For the co-localization analysis, 40% of stray light was removed with Openlabś (version 5.5.2, PerkinElmer Inc.) no-neighbor deconvolution. The Manders co-localization coefficient was assessed with FIJI (version 1.47f) co-localization tool Coloc2. STED imaging was calibrated for xy-spatial resolution using fluorescent nanobeads as detailed in suppl. Fig S2.

Ca^{2+} imaging and analysis of Jurkat-Orai1G-GECO1.2 T cells

Jurkat G-GECO1.2-Orai1 T cells were loaded with Fura2-AM (4 μM) for 30 min at 37°C. After rinsing, T cells were resuspended in Ca^{2+} buffer [140 mM NaCl, 5 mM KCl, 1 mM $MgSO_4$, 1 mM $CaCl_2$, 20 mM Hepes (pH 7.4), 1 mM NaH_2PO_4, 5 mM glucose]. As control Jurkat G-GECO1.2-Orai1 T cells were either resuspended in Ca^{2+} free buffer [140 mM NaCl, 5 mM KCl, 1 mM $MgSO_4$, 20 mM Hepes (pH 7.4), 1 mM NaH_2PO_4, 5 mM glucose, 1 mM EGTA], incubated 20 min with 100 μM Synta66 (Aobious) to pharmacologically block CRAC channels or loaded with 5 μM BAPTA-AM for 30 min. Furthermore, Jurkat G-GECO1.2-Orai1 T cells were incubated over night with 500 μM BZ194 to specifically block NAADP signaling. Cells were added on prepared coverslips and allowed to adhere before measurement. Imaging was carried out with a Leica IRBE microscope (100-fold magnification) using a Sutter DG-4 as a light source and an electron-multiplying charge-coupled device camera (C9100–13, Hamamatsu). Exposure time was 20 ms for 340 nm and 380nm and 400 ms for the G-GECO1.2 (488 nm) in 16-bit mode. The following filters were used (ex1, 340/26; ex2, 387/11; ex3, 472/30; bs, 495; em, 520/35). For functional prove of a steady-state mechanism, cells were not stimulated and transient, local Ca^{2+}entry signals were detected using four 10 × 20 pixel ROIs in each cell at the plasma membrane after background correction. Tracings of the ROIs were analyzed by ratioing F/F_0 and signals ≥ Δ 0.1 ratio units were defined as signal. To test whether the ORAI1-GECO construct worked as expected, at the end of measurements Jurkat G-GECO1.2-Orai1 T cells were stimulated with 1.67 μM thapsigargin (Calbiochem/Merck Millipore).

Statistics

All data are shown as mean ± SEM of at least three independent experiments. No specific randomization or blinding protocols were used. Figures were prepared using Matlab and Prism 5 (GraphPad Software). Different groups were compared using a two-tailed unpaired Student’s t-test, a Mann-Whitney-U-test or a Kruskal-Wallis Test using Prism5. Differences with a p value of <0.05 were considered significant: *p<0.05; **p<0.005; ***p<0.001.

Supplementary Material

Refer to Web version on PubMed Central for supplementary material.

Author Manuscript Author Manuscript Author Manuscript Author Manuscript

Acknowledgments

We are grateful to Jan Kempski (Hamburg) for help with spleen preparations and Ralf Fliegert (Hamburg) for help with supplementary movies. We thank Murali Prakriya (Chicago) and Anjana Rao (San Diego) for making available to us expression vectors for STIM1-CFP and ORAI1-YFP via addgene.

Funding

The authors acknowledge financial support by Deutsche Forschungsgemeinschaft (grant GU 360/15-2 (AHG); SFB 936/A1, Z3 (FIK); SFB1328/A01 (AHG, AF), SFB1328/A02 (IMAW, RW), SFB1328/A04 (CM), postdoctoral fellowships KA 4083/2-1 (UK) and VA 882/1-1 (MV)), Landesforschungsförderung Hamburg ReAd Me (project 1, IMAW and AHG), and NIH (grants AI097302 and AI107448 (SF), and R01NS055293 and R01NS074257 (DR)).

References and Notes

1. There is only one reference list spanning the text, figure captions and supplementary materials. Do not include a second reference list in the supplementary materials section. Reference only cited in the supplementary materials section are not counted toward length guidelines.

Note for editor: This is why there are more publications in the reference list then cited in the main text. Some publications are only cited in the supplementary materials.

1. Wolf IM, Diercks BP, Gattkowski E, Czarniak F, Kempski J, Werner R, Schetelig D, Mittrücker HW, Schumacher V, von Osten M, Lodygin D, Flügel A, Fliegert R, Guse AH, Frontrunners of T cell activation: Initial, localized Ca2+ signals mediated by NAADP and the type 1 ryanodine receptor. Sci. Signal 8(398), ra102 (2015). [PubMed: 26462735]
2. Streb H, Irvine RF, Berridge MJ, Schulz I, Release of Ca^{2+} from a nonmitochondrial intracellular store in pancreatic acinar cells by inositol-1,4,5-trisphosphate. Nature. 306, 67–69 (1983). [PubMed: 6605482]
3. Guse AH, da Silva CP, Berg I, Skapenko AL, Weber K, Heyer P, Hohenegger M, Ashamu GA, Schulze-Koops H, Potter BVL, Mayr GW, Regulation of calcium signalling in T lymphocytes by the second messenger cyclic ADP-ribose. Nature. 398, 70–73 (1999). [PubMed: 10078531]
4. Gasser A, Bruhn S, Guse AH, Second messenger function of nicotinic acid adenine dinucleotide phosphate revealed by an improved enzymatic cycling assay. J. Biol. Chem 281, 16906–16913 (2006). [PubMed: 16627475]
5. Putney JW, A model for receptor-regulated calcium entry. Cell Calcium. 7, 1–12 (1986). [PubMed: 2420465]
6. Liou J, Kim ML, Heo WD, Jones JT, Myers JW, Ferrell JE Jr, Meyer T, STIM Is a Ca^{2+} Sensor Essential for Ca^{2+}-Store-Depletion-Triggered Ca2+ Influx. Curr. Biol 15, 1235–1241 (2005). [PubMed: 16005298]
7. Feske S, Gwack Y, Prakriya M, Srikanth S, Puppel SH, Tanasa B, Hogan PG, Lewis RS, Daly M, Rao A, A mutation in Orai1 causes immune deficiency by abrogating CRAC channel function. Nature. 441, 179–185 (2006). [PubMed: 16582901]
8. Vaeth M, Yang J, Yamashita M, Zee I, Eckstein M, Knosp C, Kaufmann U, Karoly Jani P, Lacruz RS, Flockerzi V, Kacskovics I, Prakriya M, Feske S ORAI2 modulates store-operated calcium entry and T cell-mediated immunity. Nat. Commun 8, 14714 (2017). [PubMed: 28294127]
9. Wolf IMA, Guse AH Ca2+ microdomains in T-Lymphocytes. Front Oncol. 7, 73 (2017). [PubMed: 28512623]
10. Dammermann W, Zhang B, Nebel M, Cordiglieri C, Odoardi F, Kirchberger T, Kawakami N, Dowden J, Schmid F, Dornmair K, Hohenegger M, Flügel A, Guse AH, Potter BVL, NAADP-mediated Ca^{2+} signaling via type 1 ryanodine receptor in T cells revealed by a synthetic NAADP antagonist. Proc. Natl. Acad. Sci. U. S. A 106, 10678–10683 (2009). [PubMed: 19541638]
11. Dynes JL, Amcheslavsky A, Cahalan MD, Genetically targeted single-channel optical recording reveals multiple Orai1 gating states and oscillations in calcium influx. Proc. Natl. Acad. Sci 113, 440–445 (2016). [PubMed: 26712003]

Author Manuscript Author Manuscript Author Manuscript Author Manuscript

12. Calcraft PJ, Ruas M, Pan Z, Cheng X, Arredouani A, Hao X, Tang J, Rietdorf K, Teboul L, Chuang KT, Lin P, Xiao R, Wang C, Zhu Y, Lin Y, Wyatt CN, Parrington J, Ma J, Evans AM, Galione A, Zhu MX, NAADP mobilizes calcium from acidic organelles through two-pore channels. Nature 459, 596–600, 2009. [PubMed: 19387438]
13. Brailoiu E, Churamani D, Cai X, Schrlau MG, Brailoiu GC, Gao X, Hooper R, Boulware MJ, Dun NJ, Marchant JS, Patel S, Essential requirement for two-pore channel 1 in NAADP-mediated calcium signaling. J. Cell Biol 186, 201–209, 2009. [PubMed: 19620632]
14. Zong X, Schieder M, Cuny H, Fenske S, Gruner C, Rötzer K, Griesbeck O, Harz H, Biel M, Wahl-Schott C, The two-pore channel TPCN2 mediates NAADP-dependent Ca^{2+}-release from lysosomal stores. Pflugers Arch. 458, 891–899, 2009. [PubMed: 19557428]
15. Luik RM, Wu MM, Buchanan J, Lewis RS, The elementary unit of store-operated Ca^{2+} entry: local activation of CRAC channels by STIM1 at ER-plasma membrane junctions. J. Cell Biol 174, 815–825, 2006. [PubMed: 16966423]
16. Dries E, Santiago DJ, Gilbert G, Lenaerts I, Vandenberk B, Nagaraju CK, Johnson DM, Holemans P, Roderick HL, Macquaide N, Claus P, Sipido KR KR, Hyperactive ryanodine receptors in human heart failure and ischemic cardiomyopathy reside outside of couplons. Cardiovasc. Res 2018 4 14. doi: 10.1093/cvr/cvy088.
17. Awasthi S, Izu LT, Mao Z, Jian Z, Landas T, Lerner A, Shimkunas R, Woldeyesus R, Bossuyt J, Wood B, Chen YJ, Matthews DL, Lieu DK, Chiamvimonvat N, Lam KS, Chen-Izu Y, Chan JW, Multimodal SHG-2PF Imaging of microdomain Ca^{2+}contraction coupling in live cardiac myocytes. Circ. Res 118, e19–28, 2016. [PubMed: 26643875]
18. Shigetomi E, Hirayama YJ, Ikenaka K, Tanaka KF, Koizumi S, Role of Purinergic Receptor P2Y1 in Spatiotemporal Ca^{2+} Dynamics in Astrocytes. J. Neurosci 2018 2 7;38(6):1383–1395. [PubMed: 29305530]
19. Agarwal A, Wu PH, Hughes EG, Fukaya M, Tischfield MA, Langseth AJ, Wirtz D, Bergles DE, Transient Opening of the Mitochondrial Permeability Transition Pore Induces Microdomain Calcium Transients in Astrocyte Processes. Neuron 93, 587–605, 2017. [PubMed: 28132831]
20. Rungta RL, Bernier LP, Dissing-Olesen L, Groten CJ, LeDue JM, Ko R, Drissler S, MacVicar BA, Ca^{2+} transients in astrocyte fine processes occur via Ca^{2+} influx in the adult mouse hippocampus. Glia 64, 2093–2103, 2016. [PubMed: 27479868]
21. Oheim M, Schmidt E, Hirrlinger J, Local energy on demand: Are ‘spontaneous’ astrocytic Ca2+-microdomains the regulatory unit for astrocyte-neuron metabolic cooperation? Brain Res. Bull 136, 54–64, 2018. [PubMed: 28450076]
22. Brandman O, Liou J, Park WS, Meyer T, STIM2 is a feedback regulator that stabilizes basal cytosolic and endoplasmic reticulum Ca^{2+} levels. Cell. 131, 1327–1339 (2007). [PubMed: 18160041]
23. Wang X, Wang Y, Zhou Y, Hendron E, Mancarella S, Andrake MD, Rothberg BS, Soboloff J, Gill DL, Distinct Orai-coupling domains in STIM1 and STIM2 define the Orai-activating site. Nat. Commun 5, 3183, 2014 [PubMed: 24492416]
24. Miederer AM, Alansary D, Schwär G, Lee PH, Jung M, Helms V, Niemeyer BA, A STIM2 splice variant negatively regulates store-operated calcium entry. Nat. Commun 6, 6899, 2015. [PubMed: 25896806]
25. Rana A, Yen M, Sadaghiani AM, Malmersjö S, Park CY, Dolmetsch RE, Lewis RS, Alternative splicing converts STIM2 from an activator to an inhibitor of store-operated calcium channels. J. Cell Biol 209, 653–669, 2015. [PubMed: 26033257]
26. Soboloff J, Spassova MA, Hewavitharana T, He LP, Xu W, Johnstone L-S, Dziadek MA, Gill DL, STIM2 is an inhibitor of STIM1-mediated store-operated Ca2+ Entry. Curr. Biol 16, 1465–1470, 2006 [PubMed: 16860747]
27. Ong HL, de Souza LB, Zheng C, Cheng KT, Liu X, Goldsmith CM, Feske S, Ambudkar IS, STIM2 enhances receptor-stimulated Ca^{2+} signaling by promoting recruitment of STIM1 to the endoplasmic reticulum-plasma membrane junctions. Sci. Signal 8, ra3, 2015. [PubMed: 25587190]
28. Subedi KP, Ong HL, Son GY, Liu X, Ambudkar IS IS, STIM2 Induces Activated Conformation of STIM1 to Control Orai1 Function in ER-PM Junctions. Cell Rep. 23, 522–534, 2018. [PubMed: 29642009]

Author Manuscript Author Manuscript Author Manuscript Author Manuscript

29. Hohenegger M, Suko J, Gscheidlinger R, Drobny H, Zidar A, Nicotinic acid-adenine dinucleotide phosphate activates the skeletal muscle ryanodine receptor. Biochem. J 367, 423–431 (2002). [PubMed: 12102654]

30. Wang X, Zhang X, Dong XP, Samie M, Li X, Cheng X, Goschka A, Shen D, Zhou Y, Harlow J, Zhu MX, Clapham DE, Ren D, Xu H, TPC proteins are phosphoinositide-activated sodium-selective ion channels in endosomes and lysosomes. Cell 151, 372–383 (2012). [PubMed: 23063126]

31. Cang C, Zhou Y, Navarro B, Seo YJ, Aranda K, Shi L, Battaglia-Hsu S, Nissim I, Clapham DE, Ren D, mTOR regulates lysosomal ATP-sensitive two-pore Na^+ channels to adapt to metabolic state. Cell. 152, 778–790 (2013). [PubMed: 23394946]

32. Kunerth S, Langhorst MF, Schwarzmann N, Gu X, Huang L, Yang Z, Zhang L, Mills SJ, Zhang LH, Potter BVL, Guse AH, Amplification and propagation of pacemaker Ca^{2+} signals by cyclic ADP-ribose and the type 3 ryanodine receptor in T cells. J. Cell Sci 117, 2141–2149 (2004). [PubMed: 15054112]

33. Wei-Lapierre L, Carrell EM, Boncompagni S, Protasi F, Dirksen RT, Orai1-dependent calcium entry promotes skeletal muscle growth and limits fatigue. Nat. Commun 4, 2805 (2013). [PubMed: 24241282]

34. Takeshima H, Ikemoto T, Nishi M, Nishiyama N, Shimuta M, Sugitani Y, Kuno J, Saito I, Saito H, Endo M, Iino M, Noda T, Generation and Characterization of Mutant Mice Lacking Ryanodine Receptor Type 3. J. Biol. Chem 271, 19649–19652 (1996). [PubMed: 8702664]

35. Kaufmann U, Shaw PJ, Kozhaya L, Subramanian R, Gaida K, Unutmaz D, McBride HJ, Feske S, Selective ORAI1 Inhibition Ameliorates Autoimmune Central Nervous System Inflammation by Suppressing Effector but Not Regulatory T Cell Function. J. Immunol 196, 573–585 (2016). [PubMed: 26673135]

36. Oh-hora M, Yamashita M, Hogan PG, Sharma S, Lamperti E, Chung W, Prakriya M, Feske S, Rao A, Dual functions for the endoplasmic reticulum calcium sensors STIM1 and STIM2 in T cell activation and tolerance. Nat. Immunol 9, 432–443 (2008). [PubMed: 18327260]

37. Schetelig D, Wolf IMA, Diercks B-P, Fliegert R, Guse AH, Schlaefer A, Werner R, in Bildverarbeitung für die Medizin 2015, Handels H, Deserno TM, Meinzer H-P, Tolxdorff T, Eds. (Springer Berlin Heidelberg, 2015; http://link.springer.com/chapter/10.1007/9783-662-46224-9_69), Informatik aktuell, pp. 401–406.

38. Prakriy M, Feske S, Gwack Y, Srikanth S, Rao A, Hogan PG, Orai1 is an essential pore subunit of the CRAC channel. Nature. 443, 230–233 (2006). [PubMed: 16921383]

Author Manuscript Author Manuscript Author Manuscript Author Manuscript

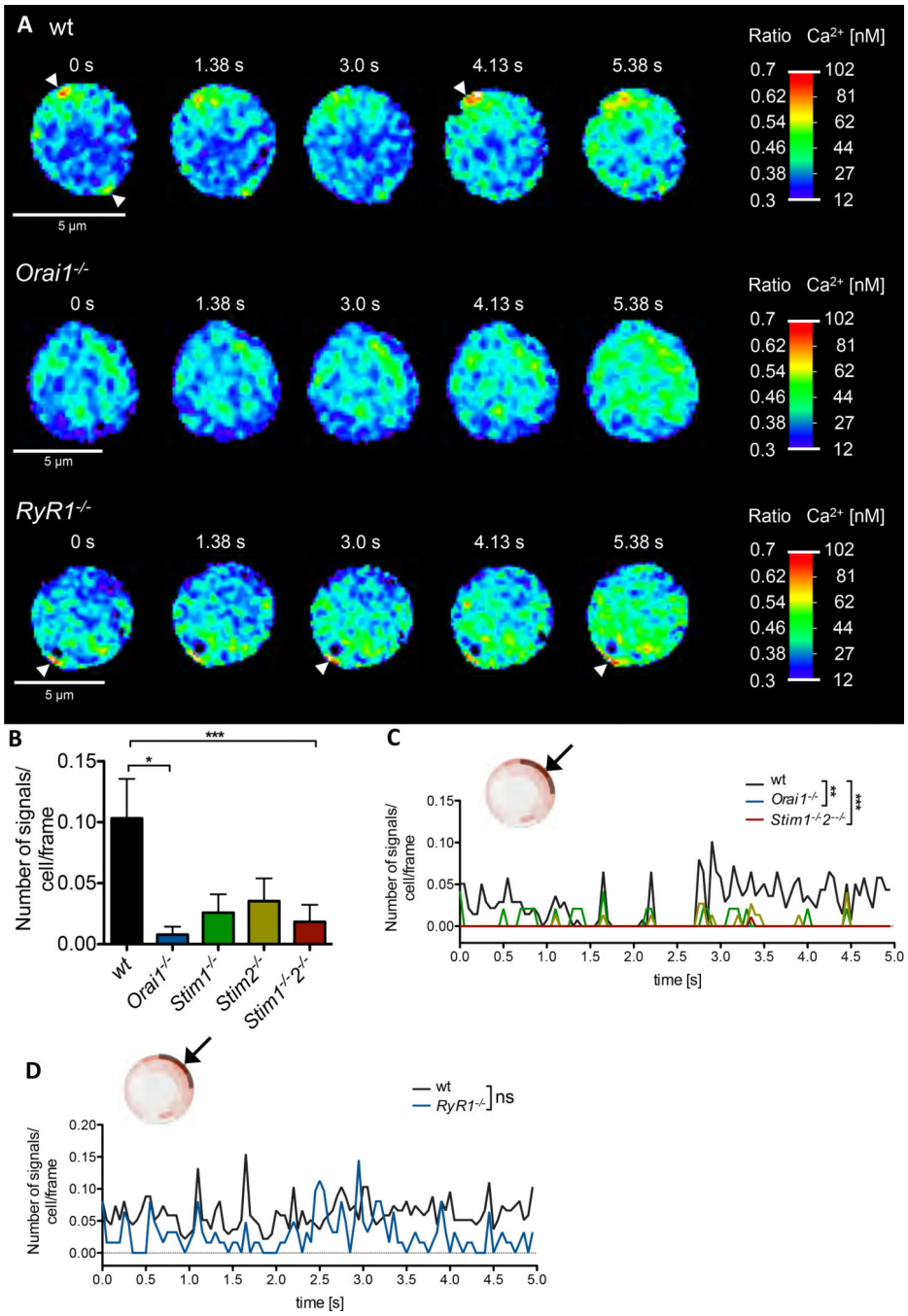

Fig. 1. Spontaneous Ca2+ microdomains in non-stimulated T cells are dependent on expression of ORAI1 and STIM1/2

(A) Ca2+ microdomains in a non-stimulated wt T cell (top), *Orai1−/−* T cell (middle) and *Ryr1−/−* T cell (bottom). Arrow heads indicate Ca2+ microdomains directly at the PM. (B) Characteristics of Ca2+ microdomains in primary murine wt (n=69), *Orai1−/−* (n=28), *Stim1−/−* (n=24), *Stim2−/−* (n=39) and *Stim1-/−2−/−* (n=46) in a 5s time period. Comparison of the number of signals per cell and frame (data represent mean ± SEM). Statistically significant differences are marked by asterisks (* p<0.05, ** p<0.01, *** p<0.001, Kruskal-Wallis Test). (C, D) Kinetic analysis of the 5s time period. Statistical

analysis was performed with wt against all other genotypes (as indicated) with Mann-Whitney-U-Test across all time points (**p<0.005, ***p<0.001).

Author Manuscript Author Manuscript Author Manuscript Author Manuscript

Author Manuscript Author Manuscript Author Manuscript Author Manuscript

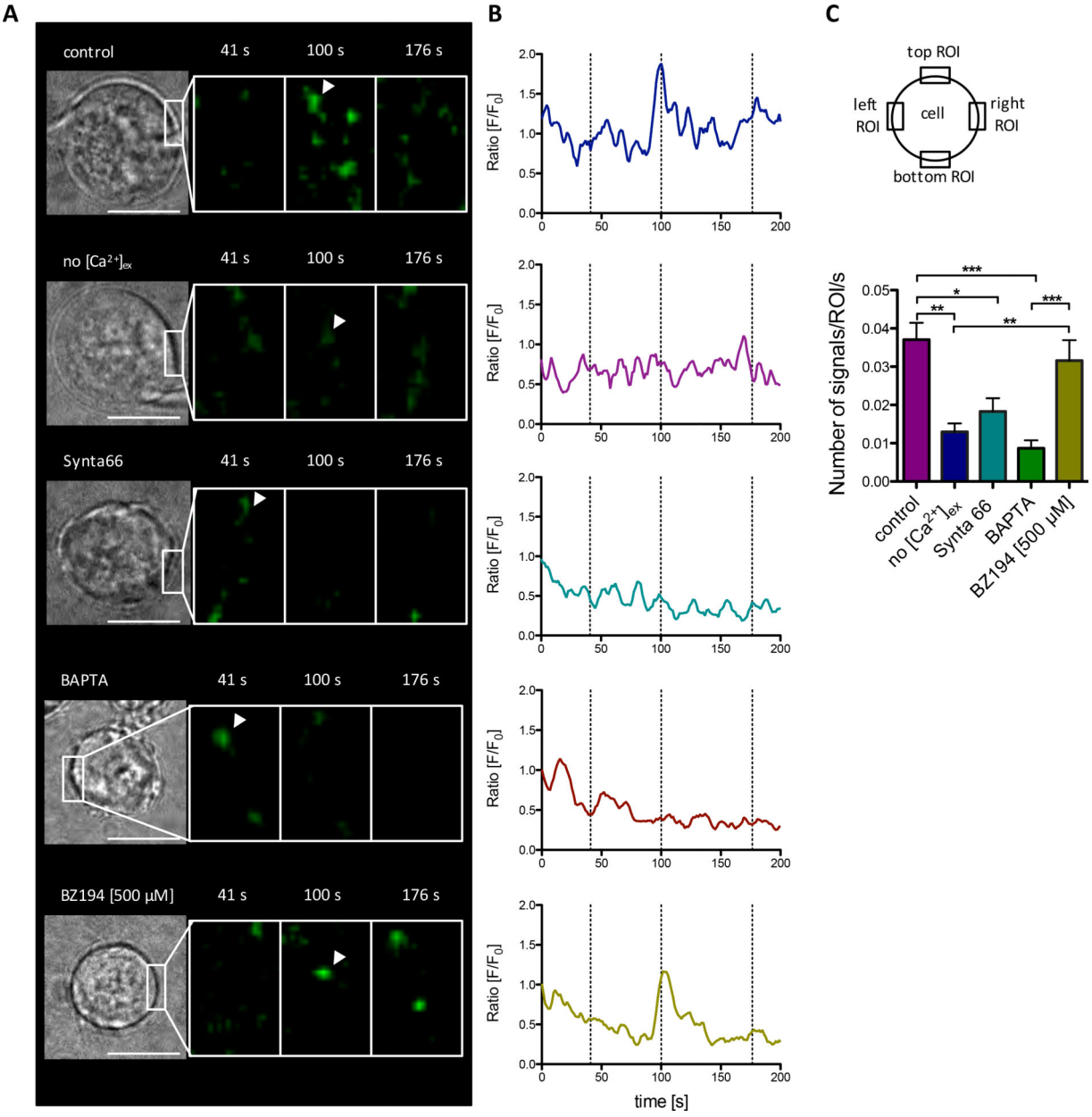

Fig. 2. Spontaneous local Ca2+ entry events via ORAI1

(A) Non stimulated Jurkat Orai1-G-GECO1.2 T cells were imaged in 1 mM Ca2+ buffer (control), in nominal Ca2+ free buffer with 1 mM EGTA (no [Ca2+]ex), or in 1 mM Ca2+ buffer containing 100 µM Synta66 (Synta66). Furthermore, Jurkat Orai1-G-GECO1.2 T cells were loaded with 5 µM BAPTA-AM or incubated with 500 µM BZ194 overnight. Indicated time points in (A) represent dashed lines in (B). (B) F/F0 tracings of ROIs (5×5 pixel) from the five representative Jurkat Orai1-G-GECO1.2 T cells in (A). Arrowheads in (A) indicate the ROIs used in (B). Noise in the tracing was reduced by a moving average filter (width=5). (C) Statistical analysis of four ROIs per cell (20 × 10 pixel) over 300 s from control (n=31), no [Ca2+]ex (n=17), Synta66 (n=18), BAPTA (n=18) and) and BZ194 (n=8). Statistically significant differences between the number of signals/ROI/s are marked

by asterisks (* $p < 0.05$, ** $p<0.01$, *** $p<0.001$, Kruskal-Wallis Test). Length scale bar in (A) represents 10 μm.

Author Manuscript Author Manuscript Author Manuscript Author Manuscript

Author Manuscript
Author Manuscript
Author Manuscript
Author Manuscript

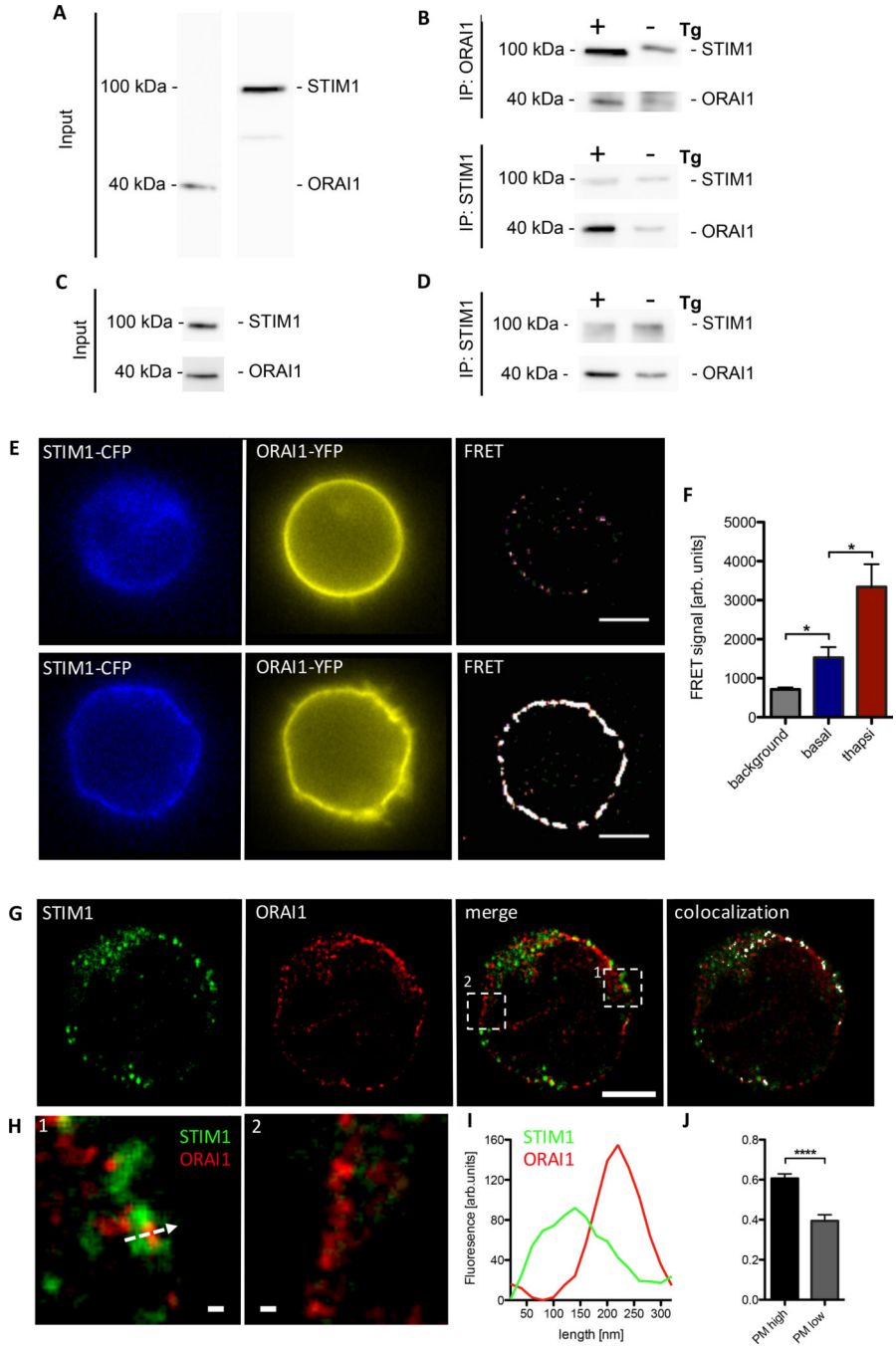

Fig. 3. ORAI1 and STIM1 form functional clusters in non-stimulated T cells

(A-D) Immunoprecipitation experiments in Jurkat T cells (A, B) and primary murine wt T cells; shown are single representative experiments from at least 3 experiments in Jurkat T cells and primary T cells. (C, D). (A) Detection of STIM1 and ORAI1 in membranes of Jurkat T cells. (B) Representative pull down of fragmented membranes obtained from non-stimulated Jurkat T cells using beads coupled with either anti-ORAI1 (top) or anti-STIM1 (bottom) (-Tg). (C) Detection of STIM1 and ORAI1 in whole cell lysates from primary murine wt T cells. (D) Pull down of fragmented membranes obtained from non-stimulated

Author Manuscript Author Manuscript Author Manuscript Author Manuscript

primary wt T cells using beads coupled with anti-STIM1 (bottom) (-Tg). As positive controls for interaction of ORAI1 and STIM1 in both Jurkat and primary murine T cells, cells were stimulated with thapsigargin (Tg) for 10 min (+Tg). (E) Representative Jurkat T cells double transfected with STIM1-CFP and ORAI1-YFP. Basal STIM CFP, ORAI1 YFP and FRET signal in non-stimulated cells (top) and after 10 min stimulation by thapsigargin (bottom) of double transfected Jurkat T cells. Length scale bar corresponds to 5 μm. (F) Statistical analysis of FRET at the plasma membrane after correction for spectral crosstalk (bleedthrough) from non-stimulated (basal n=20) and thapsigargin stimulated Jurkat cells (n=18). Background corresponds to unspecific FRET within the cytosol of both groups. Data represent mean ± SEM. Statistically significant differences are marked by asterisks (* $p<0.05$, Kruskal-Wallis Test). G to H: Co-localization of STIM1 (green) and ORAI1 (red) in a representative primary wt T cell, showing single optical channels, merge of both optical channels and co-localization (white). Length scale bar corresponds to 2 μm. (H) Magnification of a high (1) and a low (2) co-localization area of the ROIs depicted in (G); scale bar depicts 100 nm. (I) STIM1-ORAI1 plot profiles of the arrow shown in H1. (J) Statistical colocalization analysis of STIM1-ORAI1 (n=17). Data represent mean ± SEM. Statistically significant differences are marked by asterisks (**** $p<0.0001$, unpaired t test).

Author Manuscript
Author Manuscript
Author Manuscript
Author Manuscript

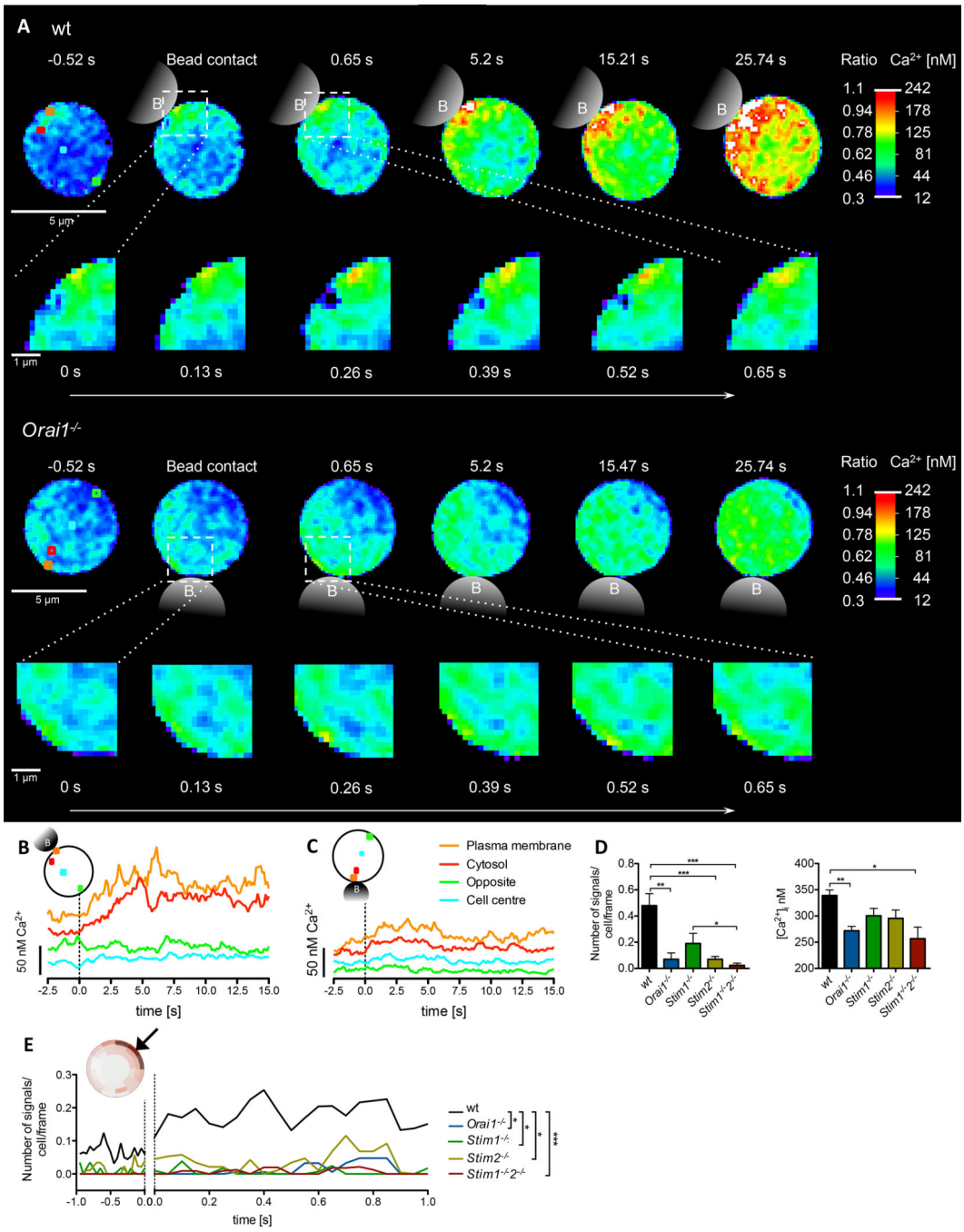

Author Manuscript
Author Manuscript
Author Manuscript
Author Manuscript

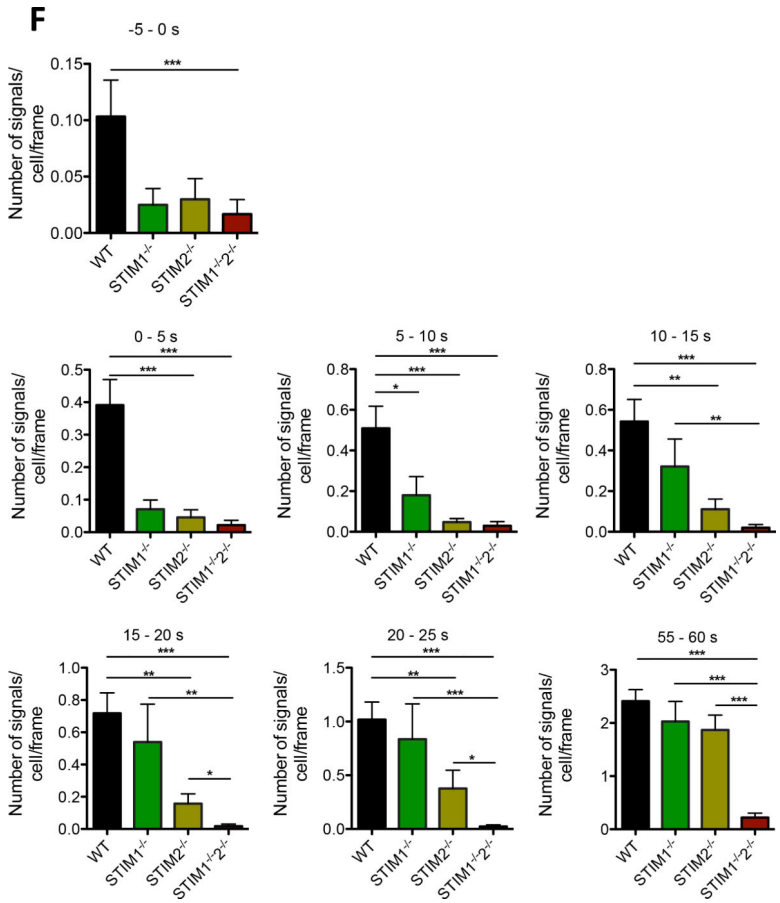

Fig. 4. *Orai1−/−*, *Stim1−/−*, and *Stim2−/−* are critical for initial Ca2+ microdomain formation upon TCR/CD28 stimulation

(A) Initial Ca2+ microdomains in a wt T cell (top) and a *Orai1−/−* T cell (bottom) upon anti-CD3/anti-CD28 stimulation (bead contact indicated schematically) and a magnified region near the bead contact site. (B, C) Respective Ca2+ tracings of four ROIs (3×3 pixel) shown in (A top; *wt*, A bottom *Orai1−/−*). Dashed line indicates time point of bead contact. (D) Characteristics of initial Ca2+ microdomains in primary murine wt (n=69), *Orai1−/−* (n=28), *Stim1−/−* (n=24), *Stim2−/−* (n=39) and *Stim1−/−/Stim2−/−* (n=46) in the first 15 s post bead contact. Comparison of the number of signals per cell and frame and the Ca2+ amplitude (data represent mean ± SEM). Statistically significant differences are marked by asterisks (* p<0.05, ** p<0.01, *** p<0.001, Kruskal-Wallis Test). (E) Primary wt, *Orai1−/−*, *Stim1−/−*, *Stim2−/−* and *Stim1−/−/Stim2−/−* T cells werestimulated by anti-CD3/anti-CD28 coated beads. Subcellular layers at the PM (as indicated) were analyzed in the first second before and post bead contact. Statistical analysis was performed with wt against all other genotypes (as indicated) with Mann-Whitney-U-Test across all time points after activation (*p<0.05, **p<0.005, ***p<0.001). (F) Ca2+ microdomain numbers were compared either before stimulation (−5s to 0s), or in 5s intervals post stimulation as indicated. Data represent mean ± SEM. Statistically significant differences between the number of signals per cell per frame are marked by asterisks (* p < 0.05, ** p<0.01, *** p<0.001, Kruskal-Wallis Test).

Author Manuscript
Author Manuscript
Author Manuscript
Author Manuscript

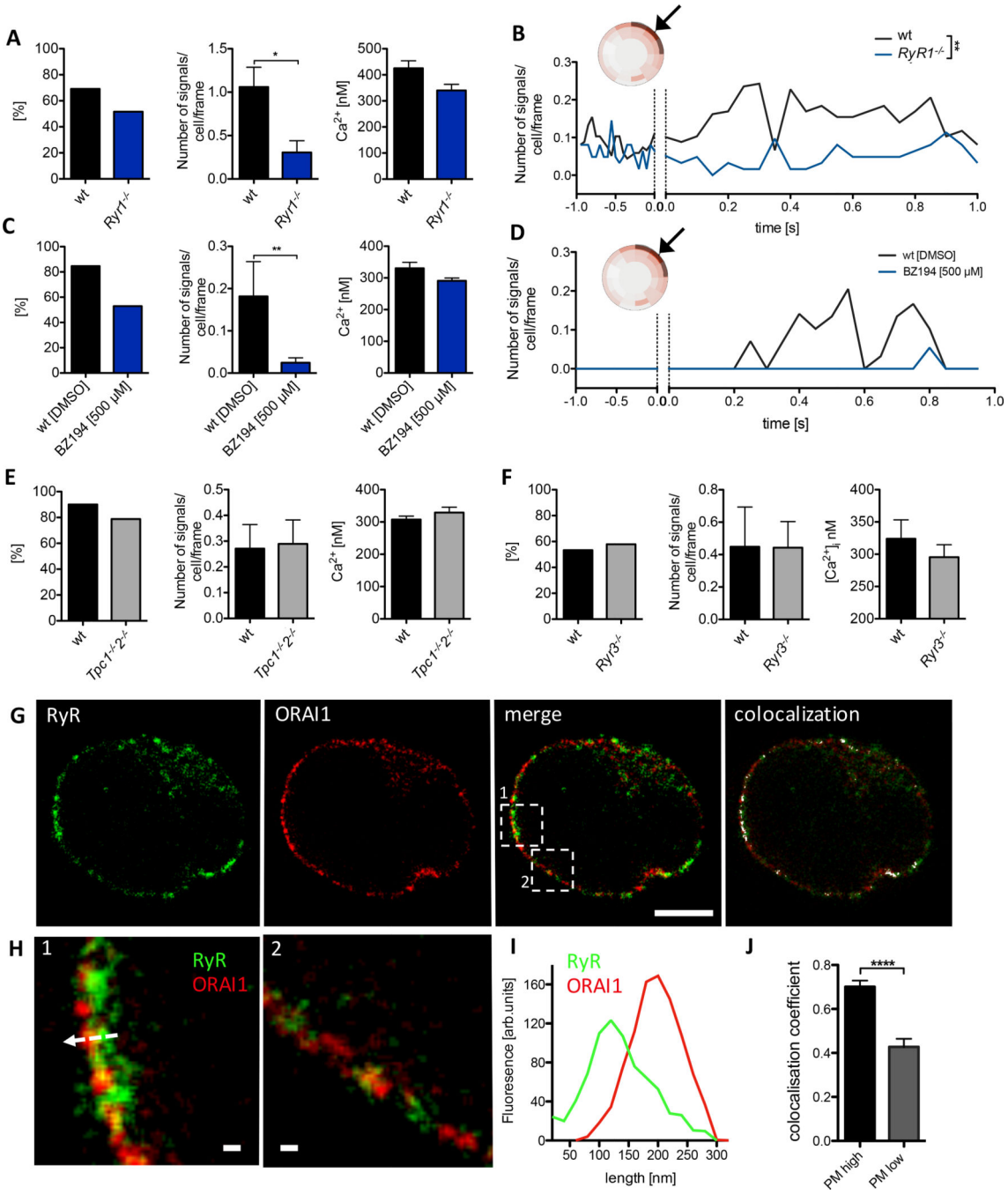

Fig. 5. RYR1, but not RYR3 or TPC1/2, as critical Ca2+ release channel for initial Ca2+ microdomains upon TCR stimulation

(A) Characteristics of initial Ca2+ microdomains in primary wt (n=68) and *Ryr1−/−* (n=31) murine T cells in the first 15 s following bead contact. (B) Subcellular layers at the PM (as indicated) were analyzed in the first second before and post bead contact. Statistical analysis was performed with wt against *RyR1−/−*, Mann-Whitney-U-Test across all time points after activation (*****p<0.05, **p<0.005, ***p<0.001). (C) Characteristics of initial Ca2+ microdomains in primary wt incubated over night with DMSO (n=13) and wt cells incubated

Author Manuscript Author Manuscript Author Manuscript Author Manuscript

over night with 500 μM BZ194 (n=34), in the first 15 s following bead contact. (C) Subcellular layers at the PM (as indicated) were analyzed in the first second before and after bead contact. (E, F) Characteristics of initial Ca2+ microdomains in (E): primary wt (n=30) and *Tpc1-/−2−/−* (n=33), and in (F): primary wt (n=15) and *Ryr3−/−* (n=19) in the first 15 s after bead contact. Comparison of the percentage of responding cells, the number of signals/cell/frame and the Ca2+ amplitude (data represent mean ± SEM). Statistically significant differences are marked by asterisks (* $p<0.05$, Mann-Whitney U). (G) Co-localization of RYR (green) and ORAI1 (red) in a representative primary wt T cell, showing single optical channels, merge of both optical channels and co-localization (white). Length scale bar corresponds to 2 μm. (H) Magnification of a high (1) and a low (2) colocalization area of the ROIs depicted in (G). Length scale bar is 100 nm. (I) RyR-ORAI1 plot profile of the arrow shown in H1. (J) Statistical co-localization analysis of RyR-ORAI1 (n=26). Data represent mean ± SEM. Statistically significant differences are marked by asterisks (**** $p<0.0001$, unpaired t test).